Volume 8, Issue 3, 2018, 3324 - 3334 ISSN 2069-5837

Biointerface Research in Applied Chemistry

www.BiointerfaceResearch.com

Original Research Article Open Access Journal

Received: 18.05.2018 / Revised: 10.06.2018 / Accepted: 12.06.2018 / Published on-line: 15.06.2018

Barrier behavior of biomedical polyurethanes: relationship of structure, morphology and properties

Aracelys Marcano [1, 2], Kateryna Fatyeyeva [1, *], Malys Koun [3], Pascal Dubuis [4], Marc Grimme [2], Stephane Marais [1]

[1]Normandie Univ., UNIROUEN, INSA ROUEN, CNRS, PBS, 76000 Rouen, France
[2]CARMAT SA, 36 Avenue de l'Europe, Immeuble l'Etendard, 78140 Vélizy Villacoublay, France
[3]ALTEN, 221bis Bd. Jean Jaurès, 92100 Boulogne-Billancourt, France
[4]INOPROD, 46 Rue de Sarlieve, 63800 Cournon D'Auvergne, France

*corresponding author e-mail address: ***kateryna.fatyeyeva@univ-rouen.fr***

ABSTRACT

Two medical grade polyurethane membranes (Chronoflex®AR-LT and Bionate®II) were studied in order to get a deeper insight into their structural and barrier properties. The results of infrared spectroscopy testify that both polyurethanes are polycarbonate- and aromatic-based. However, Chronoflex®AR-LT has a polyurethane-urea structure while Bionate®II displays a pure polyurethane structure. The thermal behavior of the membranes showed restricted chain mobility in the case of Bionate®II, resulting in the increase of the glass transition temperature compared to Chronoflex®AR-LT. The presence of the inorganic fillers (~ 9 wt.%) in Chronoflex®AR-LT was revealed as a result of the thermogravimetric analysis and scanning electron microscopy. The water and oxygen transport properties were evaluated and correlated to the polyurethane structure by the sorption and permeation measurements. The practically twice higher water and oxygen barrier properties of Bionate®II compared to Chronoflex®AR-LT suggest that the use of pure polyurethane in medical devices has significant advantages over polyurethane-urea.

Keywords: *polyurethane, Bionate, Chronoflex, morphology, transport properties*.

1. INTRODUCTION

Biomaterials play a crucial role in the tissue repair, regeneration and in the development of many medical devices [1] Therefore, a lot of research works are focused on the development of the elastomer biomaterials. Polyurethanes (PUs) are one of the widely studied synthetic elastic polymers used in the biomedical applications ranging from catheters to artificial heartcomponents [2-6] due to their diverse composition, mechanical flexibility, and mainly to their reasonably good biocompatibility [7-9]. Generally, this kind of materials is formed by the reaction of a diisocyanate, a macrodiol, and a chain extender to yield polymers containing the urethane bond (-NH-COO-). As many different monomers are now commercially available and tailor-made properties can be obtained from well-designed combinations of precursors, PUs can be tailored to meet the highly diversified demands of modern medical technologies. The polymer chains of PUs consist of alternating hard and soft segments that may lead to a two-phase morphology due to their thermodynamic incompatibility. So, the PU properties depend on the nature of the hard and soft segments, the hard segment content, and also on the nature of the chain extender [5, 10].

The chain extender agent and the diisocyanate define the hard segment structure and some physical properties. The diisocyanate insures the PU rigidity, high melting point, and crystallinity degree [11]. The chain extender agent is usually a low weight diol or diamine used to extend the length of the hard segment and to improve the hydrogen bonding between the urethane and urea groups [12]. The urethane linkages are obtained when the diols are used as the chain extenders while the diamine chain extenders react with the diisocyanate to produce the urea groups [13-15]. The PU-urea structure generally shows higher mechanical properties compared to the polyurethane structure due to the improved hydrogen bonding between the hard segments [13, 15, 16].

The soft segment consists of high molecular weight polyols (macrodiol). The most commonly used diols are polyethers and polyesters. However, PUs obtained from these polyols revealed sensitivity to the oxidative and hydrolytic degradation [17]. Therefore, other polyols were studied, for example, polycarbonate diol [14, 18]. Polycarbonate-based PU presents higher hydrolytic and thermal stability, organic solvent resistance and increased mechanical properties compared to PU-urea [13, 19-21]. Due to its better biostability, this type of polyol starts to be widely used in the applications requiring high performance properties [19, 22-24]. Reed et al. showed that after 6 months of *in vivo* implantation in rabbits, Chronoflex®AR (polycarbonate urethane) did not show any presence of microcracks, while Biomer® (polyether urethane) revealed the microcracks not only on the surface but also in the depth causing complete failure of the device [25]. Chandy et al. compared the biostability of commercially available polycarbonate urethane (Bionate®) with the stability of polyether urethane (Pellethane®) [26]. The Pellethane® tubes stored in a hydrogen peroxide and cobalt chloride solution ($H_2O_2/CoCl_2$) for 1 month showed significant surface cracking with the presence of pinholes and underwent a significant degradation after 3 months of storage (weight loss> 28%). On the contrary, the Bionate® tubes stored undersimilar conditions exhibited the surface erosion (0.25-1 μm) already during the first minutes, but without any signs of cracking or pinholes (weight loss ~ 1.8% after 10 months). Pinchuk et al.

have proved that polycarbonate urethane (Corethane™) possesses much higher resistance to the biodegradation than polyether urethane (Pellethane™ 80A) after 6 months of *in vivo* tests carried out with rabbits [13, 27]. These studies prove that polycarbonate urethanes have significant advantages of the biostability over polyether urethanes. This is probably a reason of a growing interest in the polycarbonate urethane application in biomedical fields, where the properties of these biopolymers usually compensate the cost drawback compared with "classical" polyether- or polyester-based PUs.

Because of the already mentioned thermodynamic incompatibility of more polar hard segments with less polar amorphous soft segments, the hard segments of the neighboring chains have a tendency to be self-associated by the hydrogen bonds [12, 28-31]. Hence, a phase separation takes place and micro-phase separation structures are formed. This phase separation, characteristic of segmented polyurethane, is highly dependent on the nature of the hard and soft segments, the hard segment content and the molecular weight of the soft segment [4-6, 32, 33]. It has been demonstrated that the phase separation affects the physical and functional properties of PUs, for example, permeability: the higher phase separation leads to the higher gas permeability [2, 29]. Another important parameter that should be considered during the phase separation is the mobility of the hard segment, which increases the phase separation rate [33, 34]. Also, it is shown that the longer soft segment promotes the creation of the greater domain size, thus indicating the higher phase separation [31, 33].

Sadeghi et al. have demonstrated that the phase separation leads to the increased PU rubbery properties which cause the increase of the free volume and, therefore, the permeant diffusion [2]. The replacement of polypropylene glycol by polycaprolactone (PCL) used as polyol leads to the significant decrease of the oxygen permeability (up to 60%). PCL ester groups (COO^-) can create the hydrogen bonds with the PU rigid segments, thus reducing the phase separation. Furthermore, the impact of the chain extender type on the gas permeability of the PU membranes was also highlighted [2, 29, 34]. PUs synthesized with 2,2-dimethylolpropanoic acid (DMPA) as the chain extender showed a lower permeability than those synthesized with butanediol (BDO) – $7.96 \cdot 10^{-10}$ and $4.25 \cdot 10^{-10}$ $cm^3(STP) \cdot cm \cdot cm^{-2} \cdot s^{-1} \cdot cmHg^{-1}$ for BDO and DMPA, respectively [2]. The result was attributed to a decreased phase separation due to the presence of the polar carboxylic groups in the side chains of DMPA. These findings confirm that the use of polycarbonate-based PUs has significant advantages over the use of polyether urethanes in terms of the oxygen permeability.

The choice of material for the development of biomedical devices, especially artificial hearts and ventricular assist devices (VAD), is a difficult task because the material should satisfy the numerous requirements, such as excellent biocompatibility, resistance to thrombosis (blood clotting), fatigue and degradation, and also possess the low permeability to fluids and gases [8, 35]. Usually, PUs are "the material" of choice due to their excellent mechanical properties, good blood compatibility, and ease of processing. However, like most polymers, they are known to be easily permeable towards water and gases [33, 34]. The air inlet in the prosthesis will lead to the performance and efficiency degradation and, therefore, to the lifetime decrease. On the other hand, the water permeation through the device could induce and promote the corrosion of the electric circuits, wires and other metal components inside the prosthesis. Thus, it is necessary and important to identify and select high-barrier materials for use in the biomedical devices, such as artificial hearts and VAD.

Over the years there were numerous publications and book chapters devoted to the use of PUs as biomaterials, but there are still unanswered questions about the PU permeability properties that are of great importance for the biomedical application.

Chronoflex®AR-LT is an aromatic polycarbonate-based PU synthesized from a polycarbonate polyol, a diisocyanate (methylene-bis-phenylisocyanate (MDI)) and a chain extender. This PU was formed to provide a "Low-Tack" surface, i.e. a surface with low adhesion. Bionate®II is also an aromatic polycarbonate-based PU synthesized from MDI, a chain extender and a polycarbonate polyol with C18 terminal groups.

The main aim of this work is to examine the performance of two medical grade PUs (Chronoflex®AR-LT and Bionate®II) used in the cardiovascular devices in order to correlate their water and oxygen barrier properties with the polymer structure. For that purpose, the PU chemical structure was characterized by Fourier transform infrared (FTIR) spectroscopy. The polymer morphology and thermal behavior were studied by scanning electron microscopy (SEM), atomic force microscopy (AFM) and differential scanning calorimetry (DSC) as well as thermogravimetric analysis (TGA). In addition, the influence of the temperature and the relative humidity (RH) level on the water and oxygen permeability properties was evaluated in order to provide new insights into the structure/property relationship and to identify the most suitable PU structure for the biomedical application, for example, in producing components for artificial heart and VAD.

2. EXPERIMENTAL SECTION

2.1. Materials.

Two PUs of the medical grade were used in the study, namely, Chronoflex®AR-LT supplied by AdvanSource Biomaterials (Wilmington, USA) and Bionate®II provided by DSM Biomedical (Heerlen, The Netherland). The membranes were labeled CFAR-LT for Chronoflex®AR-LT and BNII for Bionate®II. PUs were given as 10 × 10 cm^2 samples with the thickness of 300-400 μm. N_2 (99.99% purity), ultra-dry N_2 (99.99% purity, water content < 0.02 ppm) and O_2 (99.99% purity) gases were purchased from Air Products (France) and used as received. Diiodomethane and glycerol were supplied by Acros Organics™ and Alfa Aesar®, respectively. Phosphate buffered saline (PBS) solution was

supplied by VWR International S.A.S (France). Deionized water, obtained by the Millipore Milli-Q purification system (resistivity 18 MΩ·cm^{-1}), was used throughout the study.

2.2. Characterization techniques.

2.2.1. Fourier transform infrared spectroscopy (FTIR). The technique was used to identify the surface chemistry of the PU membranes. The infrared spectra were collected using the Nicolet *Avatar^{TM} 360 FTIR spectrometer* (Thermo Fisher) in the attenuated total reflectance (ATR) mode using a germanium crystal. Each spectrum was obtained by performing 100 scans with the resolution of 4 cm^{-1} over the spectral range 4000-700 cm^{-1}. Spectral manipulations, including baseline adjustment and smoothing, were performed using Omnic® software (version 5.2a).

2.2.2. Contact angle measurements. The contact angle of solvent droplets θ was measured using the Multiskop (Optrel, Germany) at room temperature (21 ± 2 °C). For each measurement, the 3 µL drop of solvent was formed at the tip of the microsyringe. After the solvent dripped onto the PU membrane, the contact angle θ was measured within 3 s by the sessile drop method with the help of CAM software. The measurements were performed on the outer and inner sides of each membrane at minimum five different locations uniformly distributed on the membrane surface and the average value of the measurements was calculated.

The hydrophobicity character of the PU membranes was evaluated using water as a liquid, whereas to determine the surface free energy, the contact angle of two other solvents (glycerol and diiodomethane) was measured.

2.2.3. Scanning electron microscopy coupled with the energy dispersive X-ray spectrometry (SEM–EDX). The morphology analysis of the PU membranes was carried out by the Carl Zeiss EVO® 40 EP scanning electron microscope equipped with the X-ray microanalyzer (Bruker) at the acceleration voltage of 15 kV. The membrane cross-sections were prepared using a surgical knife. Both surfaces and the membrane cross-sections were fixed on a carbon tape and coated with a thin layer of gold.

2.2.4. Atomic force microscopy (AFM). The surface morphology of the PU membranes was observed by AFM using the Nanoscope IIIA (Veeco – Digital Instruments, USA). The imaging process was performed in the contact mode in air at room temperature (21 ± 2 °C). The piezo-scanner used was a J-type and the used microcantilever had a resonance frequency of about 300 kHz.

2.2.5. Thermal analysis. The thermogravimetric analysis (TGA) was used in order to evaluate the thermal stability of the PU membranes. The membrane weight loss as a function of temperature was measured from 30 °C to 700 °C at the heating rate of 10 °C·min^{-1}atthe nitrogen atmosphere using the TGA Q500 system from TA Instruments (USA). The temperature modulated differential scanning calorimetry (TMDSC) experiments were performed with the TA Instruments apparatus (DSC Q 100) equipped with a low-temperature cell (minimal temperature = -70 °C). Nitrogen was used as a drying gas (70 mL·min^{-1}). The sample (about 2 mg) was encapsulated in a standard aluminium alloy pan and the pan was disposed in order to have the best possible thermal contact. Before the experiments the samples were stored in vacuum desiccators over P_2O_5 for at least two weeks to avoid moisture sorption effects. The temperature calibration was performed with benzophenone and indium standards and the energy calibration was carried out using the standard values of melting temperature (T_m) and fusion enthalpy (ΔH_m) for indium (T_m = 156.6 °C and ΔH_m = 28.66 J·g^{-1}).The specific heat capacities for each sample were measured using sapphire as a reference. TMDSC experiments were performed with the oscillation amplitude of 1.5 °C, the oscillation period of 80 s and the heating rate of 2 °C·min^{-1}. The analysis was carried out in the Heat-Only mode which is widely used for the study of crystallization and fusion processes in the semi-crystalline polymers.

2.2.6. Solvent sorption measurements. In order to determine the solvent uptake rate, the PU membranes were immersed in various solvents (water and PBS solution) at constant temperature (25 °C, 37 °C and 42 °C) till the equilibrium state (m_{eq}) was reached. The swelling degree (*SD*) was calculated from the swollen membrane mass at any time (m_t) and from the membrane dry mass (m_0) according to the following equation:

$$SD(\%) = \left(\frac{(m_t - m_0)}{m_0} \right) \cdot 100, \qquad \text{Eq. 1}$$

where m_t is the weight of the swollen membrane after removing the excess of liquid solvent from the soaked membrane surface and m_0 is the membrane dry weight obtained after membrane drying in an oven at 50 °C for 15 days.

2.2.7. Water and oxygen permeation measurements. The water permeation measurements were performed using a home-built setup[36]. The previously dried PU membrane was placed in the permeation cell and dry nitrogen was being flushed into both compartments (downstream and upstream) for hours until a dew point lower than -68 °C was obtained. Then, the upstream compartment was filled with pure deionized water. The water transfer through the membrane, i.e. from the upstream compartment to the downstream one, was monitored by measuring the increase of the dew point temperature with the chilled mirror hygrometer (Optica, General Eastern Instruments, USA). When the dew point value became constant, the steady state was considered to be reached. The experiments were conducted at atmospheric pressure (p = 1.013 bar) and three different temperatures (25 °C, 37 °C and 42 °C).

For the oxygen permeation measurements, the same experimental setup was used. However, in this case, the oxygen concentration in the downstream compartment was measured with the GPR-1600 UHP ppb O_2 analyzer (Advanced Instruments Inc., USA). As in the case of the water permeation, the cell was conditioned with dry nitrogen to remove all oxygen traces prior to testing. Then, oxygen was applied at the constant flow (560 mL·min^{-1}) in the upstream compartment. The measurements were carried out at atmospheric pressure (p=1.013 bar), at three different temperatures (25 °C, 37 °C and 42 °C) and at the RH range between 10 % and 90%.

The presented permeation results were averaged out of at least three different samples for each membrane, temperature and RH level.

3. RESULTS SECTION

3.1. Structure properties.

3.1.1. FTIR-ATR spectroscopy. The structural characterization of the PU membranes was carried out by using FTIR-ATR spectroscopy (Fig. 1). The spectra of both PU are quite similar. The symmetric N-H stretching vibrations of the urethane groups correspond to the broad absorption band near 3313 cm^{-1}, while the peak at 1593 cm^{-1} confirms the in-plane N-H bending vibration of the isocyanate segments. The absorption peaks at around 1740 cm^{-1} and 1251 cm^{-1} are characteristics of the stretching vibration of the carbonate groups C=O and the asymmetric stretching vibration of C-O(from N-CO-O), respectively [15, 37, 38]. The peak at 1058 cm^{-1} is due to the C-O-C bond stretching vibration in the urethane group. The absorption peak at 1402 cm^{-1} indicates the presence of an aromatic component in the polymer hard segment [39, 40]. This band may also serve as the reference peak for PU. The spectrum of CFAR-LT reveals the absorption peak at around 1635 cm^{-1}, which corresponds to the bonded carbonyl group [41, 42] and indicates that a diamine was used as the chain extender. The absence of this peak in the case of BNII testifies to the use of a diol as the chain extender. In addition, the peak of the bonded carbonyl group is shifted to 1702 cm^{-1} in the case of BNII, indicating a lower hydrogen bonding [40]. Indeed, the diol chain extender reacts with a diisocyanate to produce the urethane groups (Scheme 1a), while the urea groups are obtained by using a diamine as the chain extender(Scheme 1b). This fact confirms the use of different chain extenders during the PU synthesis.

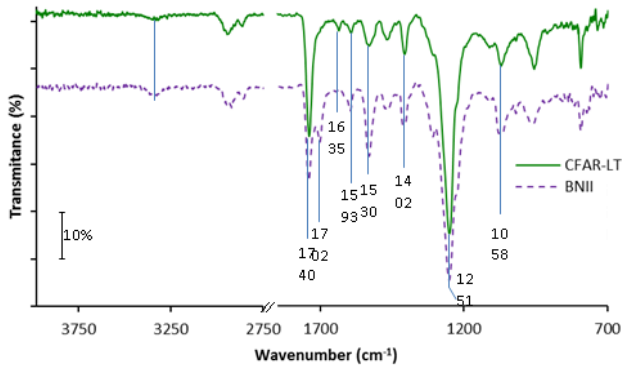

Figure 1. FTIR-ATR spectra of the PU membranes.

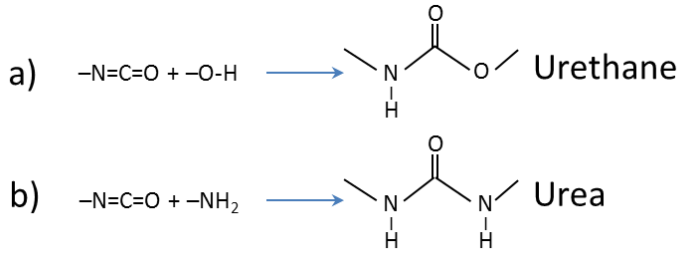

Scheme 1. Reaction between the isocyanate group and (a) diol or (b) diamine.

Generally, the presence of the urea groups in the PU structure leads to a higher content of the hydrogen bonding of the carbonyl and N-H groups compared to the content in the case of the urethane groups [12, 13, 16]. Thus, a better phase separation of the hard and soft segments should take place in CFAR-LT, thus promoting the diffusion of the small molecular species. The degree of the hydrogen bonds in the polymer can be expressed by hydrogen bond index (*HBI*) [43]:

$$HBI = \frac{A_{C=O,bonded}}{A_{C=O,free}}, \qquad \text{Eq. 2}$$

where $A_{C=O,bonded}$ and $A_{C=O,free}$ are the absorption intensity of the bonded (lower frequency) and free (higher frequency) C=O stretching vibration peaks, respectively. A slight increase of *HBI* was observed in the case of the urea linkage, i.e. for CFAR-LT, which has a higher quantity of the N-H groups in the polymer chain and, so, the improved phase separation – 1.3 and 1.1 for CFAR-LT and BNII, respectively.

3.1.2. TGA analysis. The thermal stability of the PU membranes was investigated using TGA technique (Fig. 2a). The temperatures at which 1% and 50 % weight loss occurs (T_1 and T_{50}, respectively) were calculated using the thermograms. These values can be used to evaluate the thermal stability of PUs. The thermogravimetric data are summarized in Table 1. As one can see, both PU membranes are quite thermally stable as their thermal decomposition corresponding to T_1 starts at 258 °C and 274 °C for CFAR-LT and BNII, respectively (Table 1).

A residual weight (~ 9%) at the temperature higher than 550 °C in the case of CFAR-LT can be also noted (Fig. 2a). This result can be attributed to the presence of the inorganic fillers in this PU membrane. It is generally considered that the introduction of any inorganic material into the polymer matrix can improve its thermal stability as the dispersed particles hinder the permeability of the volatile degradation products out of the material, i.e. the inorganic material generates a "barrier effect" which delays the release of the thermal degradation products in comparison with the neat polymer [44, 45]. An increase of the degradation temperature T_{50} for CFAR-LT compared to BNII, namely 359 °C and 353 °C, respectively, can be attributed to the presence of the intermolecular hydrogen bonding (a higher HBI value (1.3) compared to BNII (1.1)) as well as to the possible interactions between the inorganic fillers and the PU matrix according to [46].

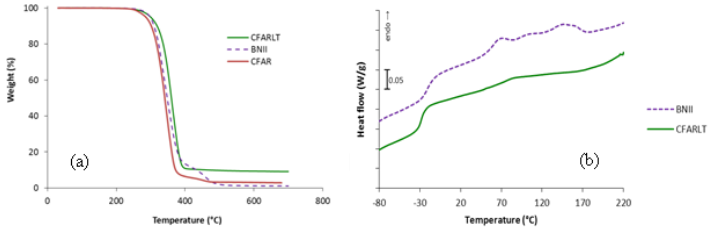

Figure 2. (a) TGA thermograms and (b) DSC curves (1st heating scan) of the studied PU membranes.

Table 1. Thermal parameters of the PU membranes obtained from TGA curves.

Membrane	Temperature of 1 % weight loss T_1(°C)	Temperature of 50 % weight loss T_{50}(°C)	Weight loss at 550°C (%)	Filler content (%)
CFAR-LT	258	359	91	9
BNII	274	353	100	-

In the case of BNII, the thermal degradation shows a two-stage process (Fig. 2a). It has been reported that the first weight loss is caused by the degradation of the hard segment as a consequence of

the relatively low thermal stability of the urethane groups (i.e. low breaking energy of C-N bond), whereas the second weight loss is associated with the soft segment decomposition [42, 44]. This implies that the hard segments are less thermally stable and that their degradation will depend on the isocyanate nature. For example, it has been noted that aromatic isocyanates are less stable than aliphatic ones [44]. The absence of the second weight loss step in the case of CFAR-LT can be explained by the presence of the inorganic fillers since for the CFAR-LT film without such a filler (labeled CFAR), the two-steps thermal degradation is clearly observed (Fig. 2a).

3.1.3.DSC analysis. The DSC curves in PUs are often difficult to interpret since many transitions occur as a result of a partial separation in the hard and soft segments. Consequently, in addition to possible crystallization processes, rearrangement of the polymer chains and breaking the physical bonds, the DSC curves may present melting and glass transition (T_g) temperatures for each of these segments. The soft segments usually possess a low T_g and a melting transition if they are semi-crystalline, while the transitions of the hard segments depend on their structure, chain length and phase mixing [41, 46].

Both PU membranes reveal a glass transition of the soft segments (T_g) (Fig. 2b). As one can see, CFAR-LT has a lower T_g value than that for BNII, namely -28.6°C and -21.3 °C, respectively. This fact indicates that a more flexible macrodiol was used for the CFAR-LT synthesis. Besides, the higher T_g value for BNII testifies to the affinity and interactions in the hard segments, which restrict the movement of the soft segments. This variation of T_g is in good agreement with the *HDI* values obtained from FTIR-ATR analysis, i.e. the lower *HDI* value for BNII. In the case of polyurethanes (i.e. for BNII), a lower number of the hydrogen bonds limits the phase separation of the hard and soft segments thus allowing the existence of a mixed structure. Such a structure provides greater polymer stiffness as the reduction of the PU chain mobility is observed thus explaining the T_g increase. On the contrary, in polyurethane-urea (i.e. for CFAR-LT), the increased number of the hydrogen bonds *HBI* is due to the presence of the urea bonds which promote the phase separation. So, the structure with well-defined hard and soft microdomains is obtained. In this case, the facilitated moving of the soft segments results in the lower T_g value.

The endothermic transition observed at about 65 °C has not been clearly defined yet [44, 45, 47-50]. According to Garret et al. this transition corresponds to the melting of the soft segments [48]. On the other hand, Choi et al. note that it cannot be attributed to the crystallization process of neither soft nor hard segments and suggest that this transition is associated to a process of a spontaneous separation between the hard and soft segments [49]. Other authors suppose that this transition may be attributed to the short-range order of the hard microdomains induced by the thermal annealing at room temperature before the measurements [43, 47, 50].

The endothermal transitions located between 100 °C and 160 °C (Fig. 2b) can be associated with different long- and short-range disruption interactions of the hard segments as well as with the interactions at the interface soft/hard microdomains, i.e. with the dissociation of the hydrogen bonds between the soft and hard segments and between the rigid microdomains as it has been reported in the literature [43, 48-51].

3.2. Surface properties.

In vivo application demands the polymers with appropriate chemical properties. These properties in the polymer surface region are even more important since the surface chemistry between blood/body tissues and the implanted medical device plays a significant role in the efficacy of the device. In addition, the analysis of the polymer surface can indicate the specific molecular alterations following the implantation. One of the first events that occur when blood is in contact with a biomaterial is the adsorption of the plasma proteins. These adsorbed proteins may induce the formation of a thrombus, which remains one of the major problems associated with the long term use of the medical devices in contact with blood. On the other hand, the presence of the micro-voids or fissures strongly enhances the diffusion of the low molecular species through the material. Consequently, the surface properties of the implanted material are critical in the biological interactions. Therefore, it is of great importance to have a deep insight into the surface properties of biomedical PU.

3.2.1. Contact angle measurements. The contact angle measurement data are gathered in Table 2. The water contact angle θ_{water} value, which is a measure of the wettability of the polymer surface, indicates that the surface of both PUs is hydrophobic in nature ($\theta_{water} \geq 90°$). Besides, the obtained results reveal that no significant difference in polarity can be observed between two membranes. The difference of the water contact angle values obtained on the membrane inner and outer surfaces of CFAR-LT and varied between 94° and 108°may be explained by the improved wettability of the inner surface. Taking into account the presence of the inorganic fillers revealed by TGA analysis (Fig. 2a and Table 1), this result may be attributed to the non-homogeneous distribution of the fillers through the membrane thickness during the film elaboration.

In order to determine the surface free energy of the PU membranes, the contact angles were also measured using two reference liquids – glycerol and diiodomethane. Based on the contact angle data, the polymer surface free energy γ_s and it's polar γ_s^p and dispersive γ_s^d components are calculated according to the Owens-Wendt approach [52] as follows:

$$\gamma_s = \gamma_s^p + \gamma_s^d \qquad \text{Eq. 3}$$

$$\gamma_L(1 + cos\theta) = 2\sqrt{\gamma_s^p \gamma_L^p} + 2\sqrt{\gamma_s^d \gamma_L^d}, \qquad \text{Eq. 4}$$

where γ_s is the surface free energy of polymer, γ_s^p and γ_s^d are the polar and dispersive components of the polymer, γ_L is the surface free energy of liquid, γ_L^p and γ_L^d are the polar and dispersive components of the liquid, θ is the contact angle value. The dispersive and polar components of water are 21.8 $mJ \cdot m^{-2}$ and 51.0 $mJ \cdot m^{-2}$, those of glycerol are 37.0 $mJ \cdot m^{-2}$ and 26.4 $mJ \cdot m^{-2}$, and those of diiodomethane are 50.8 $mJ \cdot m^{-2}$ and 0 $mJ \cdot m^{-2}$.The results of the calculation are shown in Table 2. Consistently with their hydrophobic nature, both PU membranes display a relatively low surface energy (28-31 $mJ \cdot m^{-2}$). Moreover, the largely predominant contribution to γ_s is the dispersive component γ_s^d, while the polar component γ_s^p is 0.1-1.1 $mJ \cdot m^{-2}$, which is typical of a nonpolar surface. So, these membranes should have no or very

few interactions with the polar liquids, which is thermodynamically not favorable to the sorption of the aqueous liquids thus favoring the PU moisture resistance.

Table 2. Water contact angle (θ_{water}), dispersive (γ_s^d) and polar components (γ_s^p) of the surface free energy (γ_s)of the inner and outer surfaces of the PU membranes.

Membrane	θ_{water} (°)		γ_s^d (mJ·m^{-2})		γ_s^p (mJ·m^{-2})		γ_s (mJ·m^{-2})	
	inner	outer	inner	outer	inner	outer	inner	outer
CFAR-LT	94 ± 1	108 ± 1	27.2 ± 0.6	27.6 ± 0.6	0.4 ± 0.1	0.1 ± 0.0	27.6 ± 0.7	27.7 ± 0.6
BNII	90 ± 2	90 ± 1	27.4 ± 0.4	30.4 ± 0.8	1.1 ± 0.3	0.9 ± 0.2	28.5 ± 0.7	31.3 ± 1.0

Taking all aforementioned into account, one can say that both studied PU membranes exhibit the same hydrophobic character on both sides which is required when using in VAD or artificial hearts. Such a hydrophobic character allows reducing the water solubility. However, the PU rubbery state and flexibility properties may facilitate the water diffusion which presents a risk for the recommended barrier properties of the biomaterial.

3.2.2. Morphology analysis. The morphology of the PU membranes was studied using SEM coupled with EDX. According to the obtained SEM images, the PU membranes showed a dense, continuous and symmetric morphology, owing to the low T_g value and the good film-forming capacity of PU (Fig. 3A and 3B). The presence of the inorganic fillers revealed by the TGA results (Table 1) is clearly seen on the CFAR-LT surface (Fig. 3-1). Besides, one can note the higher content of the filler particles on the membrane outer surface (Fig. 3-1A) compared with its inner surface (Fig. 3-1B). The performed EDX analysis (not shown here) confirms the filler nature – in this case, it is silica particles. This fact is in agreement with the higher water contact angle values obtained on the CFAR-LT outer surface (Table 2) – 94 ± 1 ° and 108 ± 1° for the inner and outer surfaces of the membrane, respectively. On the contrary, a much smoother structure obtained due to the absence of charges appears for the BNII membrane.

The cross-section images confirm the compact and non-porous structure of PU (Fig. 3C). In the case of the BNII membrane a wrinkled appearance can be observed (Fig. 3-2C). Stokes reported a similar surface morphology for the injection molded polyether urethanes and associated it with a post-molding shrinkage [53]. In our case, however, both membranes were elaborated by the solution casting. So, the wrinkled morphology probably can be related to the membrane structure, since in the case of BNII a part of the hard segments is surrounded by the soft domains leading to a lower phase separation compared to CFAR-LT.

AFM can be used to observe the polymer surface morphology at the nanoscale as well as to quantify the surface roughness. AFM images have confirmed the different topography of the PU membranes (Fig. 4) – a much smoother surface of BNII when compared with the CFAR-LT surface whatever the membrane surface (outer or inner) (compare Fig. 4-1 with 4-2).

In addition, the roughness of the CFAR-LT membrane is found to be higher for the outer surface (701 ± 15 nm and 130 ± 12 nm for the outer and inner surfaces, respectively) due to the presence of the inorganic fillers, which is in good agreement with SEM analysis (Fig. 3) and the results of the contact angle measurements (Table 2). It should be mentioned that the hard and soft microdomains are not obviously observed in the phase images. The phase morphology shows the patterns that correspond to the surface topography and the phase differences are connected to the topography changes in the polymer membranes.

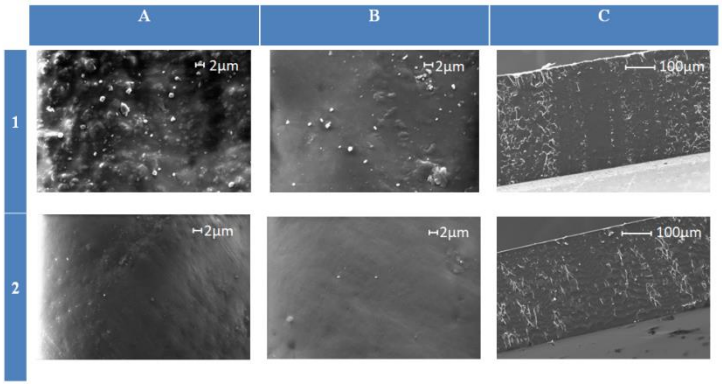

Figure 3. SEM images of (1) CFAR-LT and (2) BNII membranes: (A) outer surface, (B) inner surface and (C) cross-section.

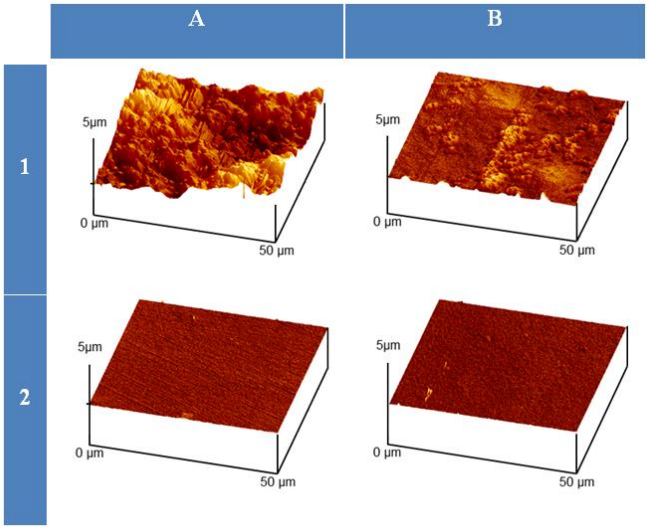

Figure 4. AFM images of (1) CFAR-LT and (2) BNII membranes: (A) outer and (B) inner surfaces.

3.3. Transport properties.

Generally, the addition of fillers to the polymer can induce a permeability reduction by increasing the diffusion path for small molecules [54]. Some authors showed a significant reduction of the gas permeability which was accompanied by a simultaneous improvement of the mechanical properties owing to adding silicate particles into the polyurethane ureamatrix [55]. The nature of the filler plays a key role in the material barrier properties. The hydrophilic fillers promote the sorption of the water molecules, which limits the efficiency of the water barrier properties. On the other hand, the filler presence in the polymer can lead to some structural changes thus increasing the permeability. A weak interaction of the filler and the polymer can improve the molecules' diffusion through the material by means of the free volume of the interfacial zones. Tirouni et al. evaluated the influence of two types of the zeolite particles incorporated in PUs for improving the separation of hydrocarbon gases [56]. The permeation of all studied gases was found to grow in the presence of the zeolite particles up to 5 wt. %. This fact was attributed to the formation of voids at the polymer/zeolite interface due to the weak interaction of the zeolite and polymer. Therefore, the free voids at the polymer/filler interface are suitable places for the diffusion and dissolution of the condensable gases such as

hydrocarbons, which results in the fact that the membrane permeability increases.

3.3.1. Sorption measurements. The water sorption measurements have revealed that CFAR-LT has a significantly higher water sorption capacity (~70% higher) than BNII whatever the studied temperature (Fig. 5). This may be explained by the polymer chemical composition and, especially, by the filler presence in the case of CFAR-LT. Indeed, the water affinity for the silica type inorganic fillers promotes the membrane water sorption.

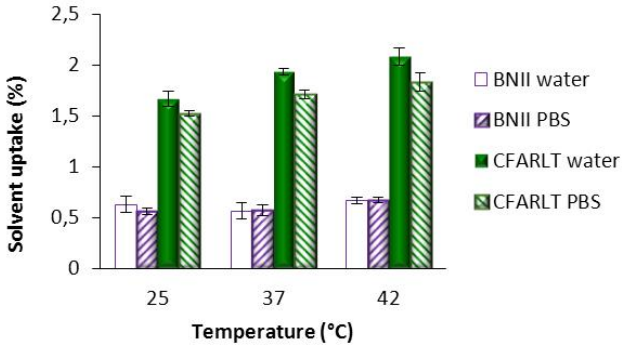

Figure 5. Water and PBS sorption capacity of the PU membranes as a function of the temperature.

When using the biomaterial, the medium which contacts PU is blood. Due to its salt composition, the PBS solution is a physiological liquid usually considered as a reference of blood. In order to be close as much as possible to the real conditions, the PU sorption capacity was tested in this physiological medium. A decrease of the sorption rate in the PBS solution compared to that in pure water was observed, especially for CFAR-LT which is more sensitive to water (Fig. 5). This fact may be explained by the presence of salts in the PBS solution that limits the water molecules to be adsorbed by the PU membrane, i.e. the presence of salts reduces the driving force by decreasing the water activity according to Raoult's law:

$$P_A = x_A \cdot P_A^*, \qquad \text{Eq. 5}$$

Where P_A is the partial pressure of the solvent vapor in the presence of a nonvolatile solute, P_A^* is the vapor pressure of the solvent in the pure state and x_A is the molar fraction, i.e the activity a_A. Therefore, it is not surprising that the water uptake is higher as compared with the values obtained in the physiological medium (Fig. 5). Since the permeability coefficient P is directly related to the solubility coefficient S, an increase of the permeability with the solubility increasing is expected. These results suggest that the introduction of a biological medium decreases the permeability of water through a polyurethane membrane in comparison with pure water.

The human body temperature can vary depending on the time of day and the level of human activity. Consequently, it was necessary to evaluate the temperature effect on the water and the PBS sorption properties of the PU membranes. The increase of the water sorption (between 2 % and 15%) with the temperature increase from 25 °C to 42 ° C was observed (Fig. 5). This increase is more visible in the case of CFAR-LT which has more affinity to water compared with BNII. The sorption increase is also observed in the case of the PBS solution. The temperature increase promotes the molecular mobility of the polymer chains that enhance the diffusion and, in some cases, the solubility of the permeant.

3.3.2. Water and oxygen permeation measurements. In order to determine the barrier performances of two studied PUs, the water and oxygen permeation measurements were performed as a function of the temperature and RH level. CFAR-LT presents the water and oxygen permeability higher than those for BNII (Table 3). The increased barrier properties of BNII may be explained by the decreased mobility of the carbonate chain in the soft segment, which results in a reduction of the free volume and, therefore, in a reduced diffusion of the permeant molecules through the polymer membrane. Thus, the lower phase separation of BNII, compared with that of CFAR-LT, can be the origin of its higher barrier properties, which is in agreement with the FTIR-ATR results, i.e. with the lower *HBI* index for BNII. Indeed, the increase of the number of the urea linkages in the polymer provokes the increase of the content of the hydrogen bonds between the hard and soft segments and, subsequently, the phase separation of the hard and soft segments. The low phase separation leads to an increase of the stiffness of some molecular chains due to the entanglement of the hard and soft segments, which causes the decrease of the chain mobility and, therefore, decreases the diffusion of the permeant molecules. The polar PU hard segments make the diffusion path more tortuous with less accessible free volume for the molecule passage and, thus, reduce the water and oxygen permeability. The absence of the silica fillers in BNII and the reduced water sorption capacity also contribute to the decrease of the water permeability.

Table 3. Water and oxygen permeability of the PU membranes at 25 °C.

Membrane	P_{H2O} (Barrer)	P_{O2} (Barrer)
CFAR-LT	7387.0±201.7	1.62±0.02
BNII	3548.9±242.1	1.14±0.01

As for the sorption measurements, the temperature effect on the permeability properties of the PU membranes was studied (Fig. 6). As expected, an increase of the water permeation flux and a decrease of the diffusion time were observed with the temperature increase due to the thermal agitation (Fig. 6a). It is known that the diffusion of the small molecules through the dense polymers occurs according to the "dissolution-diffusion" mechanism considering the presence of the available free volume and following the principle of the energy activation. Therefore, the thermal activation of the polymer chains can generate transient gaps (free volume) allowing the diffusing molecule to move from one gap to another by the successive jumps. A temperature increase induces an increase of the free volume fraction and, therefore, favors the molecular diffusion. The increase of the water permeability between 30 % and 60%with the temperature increase from 25 °C to 42°C was observed (Fig. 6b). These results are in good agreement with the water sorption capacity results (Fig. 5). As the permeability depends both on the solubility and the diffusivity, the temperature dependent diffusion coefficient was analyzed [57]. The diffusion coefficient $D_{0.24}$ was calculated from the transient regime of the permeation curve at time $t_{0.24}$ for which the flux has reached 24% of the stationary flux as follows:

$$D_{0.24} = \frac{0.091 \cdot L^2}{t_{0.24}}, \qquad \text{Eq. 6}$$

where L is the membrane thickness. As one can see, the increase of the water diffusivity with the temperature rise explains well the temperature dependence of the permeability (Fig. 6b). The similar behavior was observed in the case of the dry oxygen permeability (Fig. 6c).

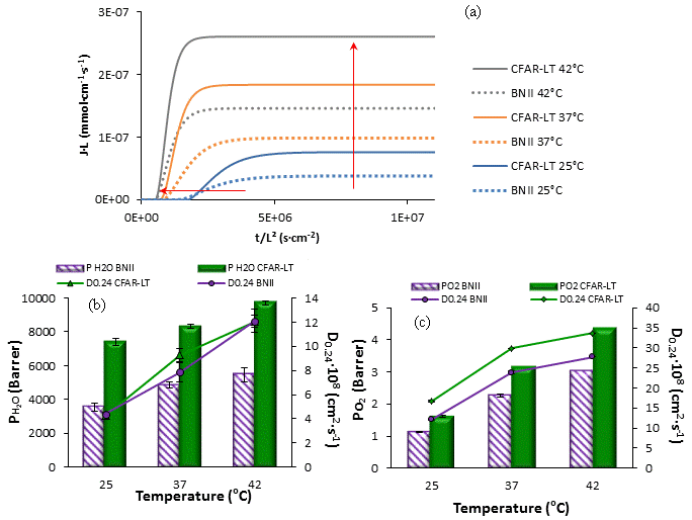

Figure 6. Effect of temperature on the (a) water permeation flux,(b)water and (c) oxygen permeability and diffusion coefficients of the PU membranes.

Water is known to affect the polymer structural properties due to the swelling effect. Some authors take into consideration the possible modifications of the polymer interface between the amorphous and crystalline phases in the presence of water [58]. Such modifications can decrease the barrier properties of the material. In the case of PUs, the presence of the absorbed water may play an important role in refining short-range order in the hard microdomains [46]. Since the human body is a very humid environment, the water plasticizing effect in PUs should be evaluated. In general, this phenomenon leads to the increase of the diffusivity and, thus, the permeability. Such a result confirms the existence of the interaction between the water molecules and the polar groups of the material by the swelling effect, i.e. by the increase of the free volume according to Scheme 2.

The plasticizing effect can be revealed by the method developed by Marais et al. [57]. This method consists in comparing the experimental water flux with a theoretical water flux (calculated assuming D constant according to Fick's law) and with a simulated flux curve (calculated using the plasticization law):

$$D = D_0 e^{\gamma C}, \qquad \text{Eq. 7}$$

where D_0 is the limit diffusion coefficient when the permeant concentration approaches zero(C=0), γ is the plasticization coefficient, and C is the local permeant concentration.

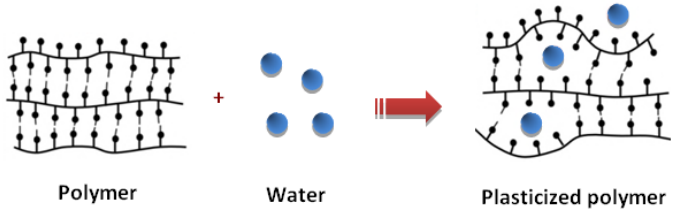

Scheme 2. Schematic representation of the water plasticizing effect.

In order to compare the diffusion behavior for all studied membranes independently of their thickness, it is necessary to normalize the curves in the same dimensionless scale of the reduced flux (J/J_{st}) versus time ($\tau_{0.24}$), where J_{st} represents the limit flux at the steady state (Fig. 7).

Fig. 7 shows an example of the water plasticizing effect for the CFAR-LT and BNII membranes at 25°C. The difference between the experimental and theoretical flux curves confirms the dependence of the diffusion coefficient on the water concentration. It can be observed that the simulated curve calculated by using the concentration-dependent diffusion coefficient (Eq. 7) fits well the experimental curve. This result clearly confirms the water plasticizing effect which enhances the water diffusivity and, thus, the water permeability.

Thus, both PU membranes are plasticized by water inducing an increase of D with C. In Table 4, the limit diffusion coefficient at nil concentration D_0 and the plasticization coefficient γC_{eq} (at $C=C_{eq}$) as a function of temperature are gathered. These data show an increase of D_0 with the temperature increase due to the thermal agitation which enhances the molecule diffusion. It can be also observed that both PU membranes are characterized by a positive plasticization coefficient γC_{eq} (Table 4). Moreover, the CFAR-LT membrane exhibits γC_{eq} values slightly higher than those for BNII whatever the temperature. The enhancement of the plasticization coefficient for the CFAR-LT membrane can be explained by its higher affinity to water (Fig. 5).

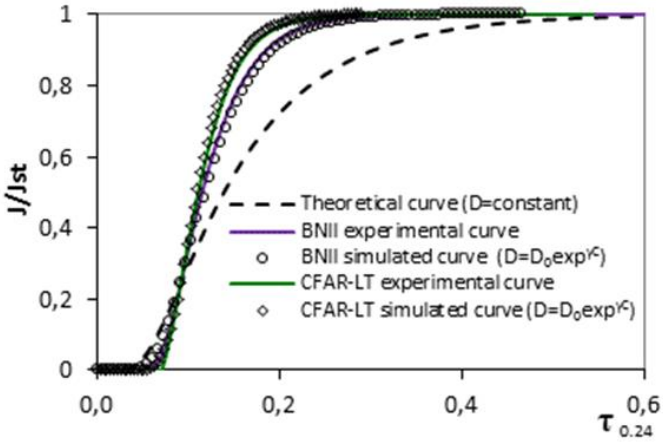

Figure 7. Experimental and simulated flux curves of the CFAR-LT and BNII membranes obtained at 25 °C.

Table 4. Limit diffusion D_0 and plasticization γC_{eq} coefficients of the PU membranes.

Temperature (°C)	CFAR-LT		BNII	
	$D_0 \cdot 10^8$ (cm²·s⁻¹)	γC_{eq}	$D_0 \cdot 10^8$ (cm²·s⁻¹)	γC_{eq}
25	1.96±0.37	2.82±0.30	2.36±0.26	2.35±0.29
37	4.25±0.66	2.67±0.22	4.61±0.27	2.12±0.16
42	5.79±0.46	2.60±0.13	6.60±0.28	2.31±0.11

Since the plasticization phenomenon is able to increase the chain segment mobility through the free volume increase, it was important to study the influence of the water plasticizing effect on the glass transition temperature. From Table 5 it can be seen that the presence of water in both PUs hydrated during 3 days decreases the T_g value due to the polymer plasticization by the water molecules thus ensuring the greater mobility of the macromolecular chains. The greater decrease of the characteristic temperature observed for CFAR-LT compared with BNII (ΔT = 4.1 °C compared to ΔT = 3.1 °C, respectively) is in good

agreement with the higher CFAR-LT water sorption capacity (Fig. 5).

Table 5. Evolution of the T_g value of the studied Pus membranes revealed by the TMDSC analysis.

Membrane	Treatment conditions	T_{g_1}(°C)
CFAR-LT	Untreated	-28.6
	hydrated during 3 days	-32.7
	dried during 7 days at 40 °C	-30.5
	dried during 7 days at 100 °C	-28.1
BNII	Untreated	-21.3
	hydrated during 3 days	-24.4
	dried during 7 days at 40 °C	-22.6
	dried during 7 days at 100 °C	-20.9

It is known that the bonded water molecules are difficult to completely remove from the polymer structure. Besides, the decrease of the T_g value observed for both PUs membranes indicates the improved phase separation between the soft and hard microdomains. In order to check the structure influence on the T_g value, the drying step was prolonged up to 7 days at 100°C (Table 5). One can note the increase of the T_g value for both membranes. This fact means that the water molecules have a strong impact on the hard segment mobility. A comparison of the T_g values obtained for the dried and hydrated membranes gives evidence of the fact that the water presence may facilitate the refinement of the hard microdomains.

The plasticizing effect is known to be reversible. The water permeation measurements were repeated five times for the same sample and the PU membranes were dried during one week over P_2O_5between each cycle (from 1st to 4th cycles). After four cycles the progressive water permeability increase might be observed (Table 6). Besides, that increase was much more pronounced for CFAR-LT which is more water permeable. Also, an increase of the plasticization coefficient γC_{eq} with the number of cycles might be noted, indicating the presence of the water molecules in the PU membrane. However, the strong drying of the PU membrane in the presence of the drying agent (P_2O_5) during 9 months (5th cycle) led to the water permeability value decreasing and its approaching to the initial permeability value (Table 6). These results confirm the reversibility of the plasticization phenomenon and reveal the absence of the hydrolysis reaction.

Table 6. The water permeability coefficient values for the PU membranes as a function of number of cycles at 25°C.

Membrane	Coefficient	Cycle				
		1	2	3	4	5
CFAR-LT	P_{H2O} (Barrer)	5861.9	6747.6	7192.3	8211.8	6705.0
	γC_{eq}	3.06	3.23	3.24	4.72	3.03
BNII	P_{H2O} (Barrer)	3631.9	3989.9	4145.7	4496.6	3406.7
	γC_{eq}	2.12	2.19	2.41	2.30	2.10

In some cases, the water plasticizing effect causes the reduction of the oxygen barrier properties, for example for the ethylene vinyl alcohol (EVOH) films [59]. For this reason, the influence of the moisture content on the oxygen permeability of the PU membranes was also evaluated. As it can be seen from Fig. 8, the oxygen permeability coefficient increases with the temperature increase. However, the oxygen permeability is not affected by the humidity level in the case of both PUs indicating that the water plasticization of PU is not sufficient enough to increase the free volume fraction and, so, to facilitate the oxygen transfer through the membrane. Thus, both studied PU membranes are of great interest to be used as a biomaterial, where the oxygen barrier properties are required.

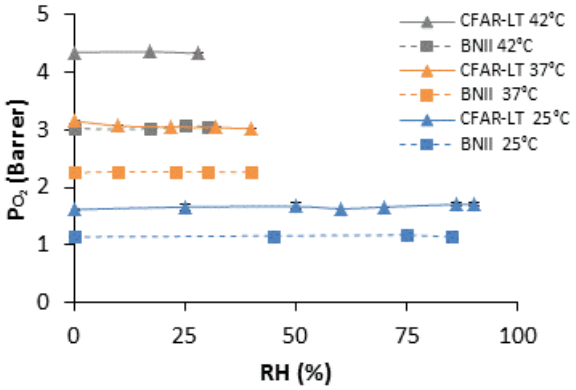

Figure 8. Effect of the RH level on the oxygen permeability coefficient of the PU membranes.

4. CONCLUSIONS

Polyurethanes find an application in various fields as they offer a wide range of compositions, properties, and complex structures. So, two medical grade polyurethane membranes (CFAR-LT and BNII) were studied in order to correlate their physical and chemical properties with their barrier behavior. It is found that due to the polyurethane-urea structure of CFAR-LT, the better phase separation of the hard and soft segments is observed as the macromolecular chains present a higher mobility. The presence of the hydrophilic inorganic fillers (~ 9 wt.%) in the CFAR-LT membrane allows us to noticeably increase its water sorption capacity, i.e. ~ up to 70% higher than in the case of BNII. It is noted that CFAR-LT has significantly lower water and oxygen barrier properties than the BNII membrane. This fact may be explained by the lower chain mobility of the soft segments and by the phase separation. The diffusion and permeability coefficients are found to grow up with the temperature increase from 25 °C to 42 °C. In addition, the water sorption decreases as compared with deionized water when the physiological (PBS) medium is used. The water plasticizing effect in PUs is revealed due to the increased chain mobility and water permeability. However, the membrane initial characteristics in terms of permeability and plasticization coefficients were obtained after the prolonged drying step proving that the plasticization is a reversible process. Moreover, no effect of the humidity level on the oxygen permeability was found for both studied membranes.

The obtained results imply that BNII (i.e. pure polyurethane) possesses the best performance in terms of the water and oxygen barrier properties making it a suitable material to be used where the water barrier properties are required.

5. REFERENCES

[1] Chen Q., Liang S., Thouas G.A., Elastomeric biomaterials for tissue engineering, *Progress in Polymer Science*, 38, 584-671, **2013**.

[2] Sadeghi M., Semsarzadeh, M.A., Barikani M., Ghalei, B., Study on the morphology and gas permeation property of polyurethane membrane, *Journal of Membrane Science*, 385-386, 76-85, **2011.**

[3] Poręba R., Špírková M., Brožová L., Lazić N., Pavličević J., Strachota A., Aliphatic polycarbonate-based polyurethane elastomers and nanocomposites. II. Mechanical, thermal, and gas transport properties, *Journal of Applied Polymer Science*, 127, 329-341, **2013**.

[4] Takahara A., Coury A., Hergenrother R., Cooper S., Effect of soft segment chemistry on the biostability of segmented polyurethanes. I. In vitro oxidation, *Journal of Biomedical Materials Research*, 25, 341-356, **1991**.

[5] Desai S., Thakore I., Sarawade B., Devi S., Effect of polyol and diisocyanates on thermomechanical and morphological properties of polyurethanes, *European Polymer Journal*, 36, 711-725, **2000**.

[6] Frontini P.M., Rink M., Pavan A., Development of polyurethane engineering thermoplastics. II. Structure and properties, *Journal of Applied Polymer Science*, 48, 2023-2032, **1993**.

[7] Stokes K., McVenes R., Polyurethane elastomer biostability, *Journal of Biomaterials Applications*, 9, 321-354., **1995.**

[8] Lelah M.D., Cooper S.L., *Polyurethanes in medicine*, CRC Press: Boca Raton, **1986**.

[9] Baheiraei N., Yeganeh H., Ai J., Gharibi R., Azami M., Faghihi F., Characterization and antioxidant activity of a novel electroactive and biodegradable polyurethane for cardiac tissue engineering application, *Materials Science and Engineering: C*, 44, 24-37, **2014**.

[10] Zdrahala R.J., Gerkin R.M., Hager S.L., Critchfield F.E., Polyether-based thermoplastic polyurethanes. I. Effect of the hard-segment content, *Journal of Applied Polymer Science*, 25, 2041-2050, **1979**.

[11] Woods G., *The ICI Polyurethanes Book*, 2nd ed.; John Wiley and Sons: New York, **1990**.

[12] Christenson E., Anderson J., Hiltner A., Biodegradation mechanisms of polyurethane elastomers, *Corrosion Engineering Science and Technology*, 42, 312-323, **2007.**

[13] Pinchuk L., A review of the biostability and carcinogenicity of polyurethanes in medicine and the new generation of biostable polyurethanes, *Journal of Biomaterials Science, Polymer Edition*, 6, 225-267, **1995**.

[14] Cauich-Rodríguez J.V., Chan-Chan L.H., Hernandez-Sánchez F., Cervantes-Uc J.M., Degradation of polyurethanes for cardiovascular applications, in *Advances in Biomaterials Science and Biomedical Applications*, Pignatello, R., Ed.; InTech, chapter 3, **2013**.

[15] Christenson E., Dadsetan M., Wiggins M., Anderson J., Hiltner A., Poly(carbonate urethane) and poly(ether urethane) biodegradation: in vivo studies, *Journal of Biomedical Research, Part A*, 69, 407-416, **2004**.

[16] Lambda N., Woodhouse K., Cooper S. *Polyurethanes in biomedical applications*, CRC Press: Boca Raton, FL, **1998**.

[17] Anderson J., Hiltner A., Wiggins M., Schubert M., Collier T., Kao W., Mathur A., Recent advances in biomedical polyurethane biostability and biodegradation, *Polymer International*, 46, 163-171, **1998**.

[18] Vermette P., Griesser H., Laroche G., Guidoin R., *Biomedical applications of polyurethanes*, Landes Biosciences, Eds.; Gerorgetown, Texas, p. 1-19, **2001**.

[19] Eceiza A., Martin M., de la Caba K., Kortaberria G., Gabilondo N., Corcuera M., Mondragon I., Thermoplastic polyurethane elastomers based on polycarbonate diols with different soft segment molecular weight and chemical structure: mechanical and thermal properties, *Polymer Engineering & Science*, 48, 297-306, **2008**.

[20] Harris R.F., Joseph M.D., Davidson C., Polyurethane elastomers based on molecular weight advanced poly(ethylene ether carbonate) polyols. IV. Effects of poly(propylene glycol) modified diols, *Journal of Applied Polymer Science*, 46, 1843-1857, **1992.**

[21] Kuran W., Sobczak M., Listos T., Debek C., Florjanczyk Z., New route to oligocarbonate diols suitable for the synthesis of polyurethane elastomers, *Polymer*, 41, 8531-8541, **2000.**

[22] Martin D.J., Meijs G.F., Renwick G.M., Gunatillake P.A., McCarthy S.J., Effect of soft segment CH_2/O ratio on morphology and properties of a series of polyurethane elastomers, *Journal of Applied Polymer Science*, 60, 557-571, **1996**.

[23] Tanaka H., Kunimura M., Mechanical properties of thermoplastic polyurethanes containing aliphatic polycarbonate soft segments with different chemical structures, *Polymer Engineering & Science*, 45, 1333-1349, **2002**.

[24] Lee D.K., Tsai H.B., Tsai R.S., Chen P.H., Preparation and properties of transparent thermoplastic segmented polyurethanes derived from different polyols, *Polymer Engineering & Science*, 47, 695-701, **2007.**

[25] Reed A., Potter J., Szycher M., A solution grade biostable polyurethane elastomer: ChronoFlex AR, *Journal of Biomaterials Application*, 8, 210-236, **1994**.

[26] Chandy T., Van Hee J., Nettekoven W., Johnson J., Long-term in vitro stability assessment of polycarbonate urethane micro catheters: resistance to oxidation and stress cracking, *Journal of Biomedical Research, Part B*, 89, 314-324, **2009**.

[27] Pinchuk L., Crack-resistant polycarbonate urethane polymer prostheses, US Patent 5133742, **1992**.

[28] Prisacariu C., *Polyurethane elastomers, from morphology to mechanical aspects*, Springer-Verlag/Wien, Eds. New York, p. 3-22, **2011**.

[29] Mondal S., Hu J., Segmented shape memory polyurethane and its water vapor transport properties, *Designed Monomers and Polymers*, 9, 527-550, **2006**.

[30] Chen Q., Liang S., Thouas G., Elastomeric biomaterials for tissue engineering, *Progress in Polymer Science*, 38, 584-671, **2013**.

[31] Velankar S., Cooper S.L., Microphase separation and rheological properties of polyurethane melts 2. Effect of block incompatibility on the microstructure, *Macromolecules*, 33, 382-394, **2000**.

[32] Zha L., Wu M., Yang J., Hydrogen bonding and morphological structure of segmented polyurethanes based on hydroquinone- bis(p-hydroxyethyl)ether as a chain extender, *Journal of Applied Polymer Science*, 73, 2895-2902, **1999**.

[33] O'Sickey M.J., Lawrey B.D., Wilkes G.L., Structure–property relationships of poly(urethane urea)s with ultra-low monol content poly(propylene glycol) soft segments. I. Influence of soft segment molecular weight and hard segment content, *Journal of Applied Polymer Science*, 84, 229-243, **2002**.

[34] McGee M.G., Szycher M., Turner S.A., Clay W., Trono R., Fuqua F., Norman J.C., Use of a composite Biomer-butyl rubber/Biomer material to prevent transdiaphragmatic water permeation during long-term, electrically-actuated left ventricular assist device (LVAD) pumping, *Transactions – American Society for Artificial Internal Organs*, 26, 299-303, **1980**.

[35] McMillin C.R., Physical testing of polymers for use in circulatory assist devices, *Artificial Organs*, 7, 78-91, **1983**.

[36] Métayer M., Labbé M., Marais S., Langevin D., Chappey C., Dreux F., Brainville M., Belliard P., Diffusion of water through various polymer membranes: a new high performance method of characterization, *Polymer Testing*, 18, 533-549, **1999**.

[37] Zhang Z., King M.W., Guidoin R., Therrien M., Pezolet M., Adnot A., Ukpabi P., Vantal M.H., Morphological, physical and chemical evaluation of the Vascugraft® arterial prosthesis: comparison of a novel polyurethane device with other microporous structures, *Biomaterials*, 15, 483-501, **1994**.

[38] Dempsey D.K., Carranza C., Chawla C.P., Gray P., Eoh J.H., Cereceres S., Cosgriff-Hernandez E.M., Comparative analysis of in vitro oxidative degradation of poly(carbonate urethanes) for biostability screening, *Journal of Biomedical Research, Part A*, 102, 3649-3665, **2014**.

[39] Dillon J., *Infrared Spectroscopic Atlas of Polyurethanes*, Lancaster, PA: Technomic Publication, **1989**.

[40] Xie X., Tan H., Li J., Zhong Y., Synthesis and characterization of fluorocarbon chain end-capped poly(carbonate urethane)s as biomaterials: a novel bilayered surface structure, *Journal of Biomedical Research, Part A*, 84, 30-43, **2008**.

[41] Sung C.S.P., Smith T.W., Sung N.H., Properties of segmented polyether poly(urethaneureas) based of 2,4-toluene diisocyanate. 2. Infrared and mechanical studies, *Macromolecules*, 13, 117-121, **1980**.

[42] Yang J.H., Chun B.C., Chung Y.C., Cho J.H., Comparison of thermal/mechanical properties and shape memory effect of polyurethane

block-copolymers with planar or bent shape of hard segment, *Polymer*, 44, 3251-3258, **2003**.
[43] Sadeghi M., Semsarzadeh M.A., Barikani M., Ghalei B., The effect of urethane and urea content on the gas permeation properties of poly(urethane-urea) membranes, *Journal of Membrane Science*, 354, 40-47, **2010**.
[44] Coutinho F., Delpech M., Alves T., Ferreira A., Degradation profiles of cast films of polyurethane and poly(urethane-urea) aqueous dispersions based on hydroxyl-terminated polybutadien and different diisocyanate, *Polymer Degradation and Stability*, 81, 19-27, **2003**.
[45] Moon S.Y., Kim J.K., Nah C., Lee Y.S., Polyurethane/montmorillonite nanocomposites prepared from crystalline polyols, using 1,4-butanediol and organoclay hybrid as chain extenders, *European Polymer Journal*, 40, 1615-1621, **2004**.
[46] Xiong J., Zheng Z., Jiang H., Ye S., Wang X., Reinforcement of polyurethane composites with an organically modified montmorillonite, *Composites, Part A*, 38, 132-137, **2007**.
[47] Saiani A., Daunch W.A., Verbeke H., Leenslag J.W., Higgins J.S., Origin of multiple melting endotherms in a high black content polyurethane. 1. Thermodynamic investigation, *Macromolecules*, 34, 9059-9068, **2001**.
[48] Garret J.T., Xu R., Cho J., Runt J., Phase separation of diamine chain-extended poly(urethane) copolymers: FTIR spectroscopy and phase separations, *Polymer*, 44, 2711-2717, **2003**.
[49] Choi T., Weksler J., Padsalgikar A., Runt J., Influence of soft segment composition on phase-separated microstructure of polydimethylsiloxane-based segmented polyurethane copolymers, *Polymer*, 50, 2320-2327, **2009**.
[50] Isfahani A.P., Sadeghi M., Dehaghai A.H.S., Aravand M.A., Enhancement of the gas separation properties of polyurethane membrane by epoxy nanoparticles, *Journal of Industrial and Engineering Chemistry*, 44, 67-72, **2016**.
[51] Chen T.K., Shieh T.S., Chui J.Y., Studies on the first DSC endotherm of polyurethane hard segment based on 4,4′-diphenylmethane diisocyanate and 1,4-butanediol, *Macromolecules*, 31, 1312-1320, **1998**.
[52] Rudawska A., Jacniacka E., Analysis for determining surface free energy uncertainty by the Owen-Wendt method, *International Journal of Adhesion and Adhesives*, 29, 451-457, **2009**.
[53] Stokes K.B., Polyether polyurethanes: biostables or not? *Journal of Biomaterials Application*, 3, 228-259, **1988**.
[54] Bharadwaj R.K., Modeling the barrier properties of polymer-layered silicate nanocomposites, *Macromolecules*, 34, 9189-9192, **2001**.
[55] Xu R., Manias E., Snyder A.J., Runt J., New biomedical poly(urethane-urea)-layered silicate nanocomposites, *Macromolecules*, 34, 337-339, **2001**.
[56] Tirouni I., Sadeghi M., Pakizeh M., Separation of C_3H_8 and C_2H_6 from CH_4 in polyurethane–zeolite 4Å and ZSM-5 mixed matrix membranes, *Separation and Purification Technology*, 141, 394-402, **2015**.
[57] Marais S., Métayer M., Nguyen Q.T., Labbé M., Langevin D., New methods for the determination of the parameters of a concentration-dependent diffusion law for molecular penetrants from transient permeation or sorption data, *Macromolecular Theory and Simulations*, 9, 207-214, **2000**.
[58] Bastioli C., Guanella I., Romano G., Effects of water sorption on the physical properties of PET, PBT, and their long fibers composites, *Polym. Compos*., 11, 1-9, **1990.**
[59] Zhang Z., Britt I.J., Tung M.A., Permeation of oxygen and water vapor through EVOH films as influenced by relative humidity, *Journal of Applied Polymer Science*, 82, 1866-1872, **2001**.

6. ACKNOWLEDGEMENTS

The authors would like to thank ANRT (French Ministry-CIFRE n° 2014/0632) for the financial support of this research, J. Gonand (M2C UMR 6143, Rouen University) and Dr. J.-M. Valleton (PBS UMR 6270, Rouen University) for the SEM and AFM measurements, respectively, and Dr. A. Esposito (GPM UMR 6634, Rouen University) for TMDSC assistance and helpful discussions.